AIAA JOURNAL
Vol. 41, No. 10, October 2003

Influences of Blade Bowing on Flowfields of Turbine Stator Cascades

Chunqing Tan* and Atsumasa Yamamoto†
National Aerospace Laboratory of Japan, Tokyo 182-8522, Japan
Shinpei Mizuki‡
Hosei University, Tokyo 184-8584, Japan
and
Haisheng Chen§
Chinese Academy of Sciences, 100080 Beijing, People's Republic of China

To understand the influences of blade positive and negative bowing on flowfields of turbine stator cascades with low aspect ratio, six sets of cascades with different bowed angles of the blades were designed and tested. A five-hole pitot microprobe, which was located upstream and downstream of the cascades, was used to survey the flowfields in detail. The results were different from other published results with a different kind of turbine stator blade profile. When a blade has positive or negative bowing, the passage vortices do not change, whereas the characteristics of the trailing vortices, such as the intensity, locations, size, and structure, do change distinctly. In the case of blade positive bowing, the local spanwise distribution of the yaw flow angle at the cascade exit is significantly affected, with very little changes in the cascade overall loss.

Introduction

In the past two decades, many researchers, such as Langston et al.,[1] Sieverding,[2] Moore and Adhye,[3] and Yamamoto,[4,5] have demonstrated secondary flow mechanisms in turbine cascades. They showed that the secondary flow has a complex structure, and they believed that associated secondary flow losses are generated and determined by the secondary flows themselves. To reduce secondary losses, the bowed blade, the concept of which was published in the 1960s by Deich et al.,[6] has attracted great attentions by many well-known researchers, such as Wang et al.[7–9] Shi et al.,[10] Harrison,[11] Han et al.,[12] Wallis and Denton,[13] and Chen et al.[14]

In the turbine stator cascades with low aspect ratio, the losses near the cascade endwalls contribute the most to the overall cascade loss. Therefore, it is a common sense to reduce the losses near the endwalls to reduce the overall cascade loss. A detailed experimental study with a kind of turbine stator blade profile[9] was performed to reveal the influences of blade "positive" bowing on the cascade flowfields. Positive bowing is defined as an acute dihedral angle between the pressure side of the blade and cascade endwalls. The experiment was carried out using linear turbine stator cascades of low aspect ratio, so that the positive bowing would create a C-shape spanwise static pressure distribution on the blade surfaces, particularly on the blade suction surface. The C-shape distribution leads the low-energy fluids near the endwalls to roll up toward the midspan more intensely compared to the straight blade without bowing and, hence, greatly decreases the loss near the endwalls. They found an optimum bowed angle of about 20 deg, which would reduce the straight cascade loss by up to 40%. This optimum bowed angle also corresponds to the angle at which the overall cascade loss is at a minimum. Up to now, the result mentioned has been widely applied to all linear turbine stator cascades with low aspect ratio. The result has also been used in the practical design and application of gas and steam turbines (with low-aspect-ratio blades).

Note that the preceding results came only from experiments using one kind of turbine stator blade profile (here called Wang's turbine stator blade profile). Thus, it is absolutely necessary to verify its adaptability by obtaining more experimental data with other kinds of blade profiles. In addition, because up to now there are no detailed results on the influence of blade negative bowing, the present paper will provide additional data for a different blade profile, obtained experimentally with six sets of cascades with both positive and negative bowings.

Experimental Method

A series of experiments were conducted with the low-speed linear cascade wind tunnel of the National Aerospace Laboratory of Japan (NAL) as shown in Fig. 1. Atmospheric air is sucked through a bellmouth by a dc blower located far downstream of the test cascade. The wind tunnel has two large vertical semicircular cascade endwalls in between which a test cascade is installed. One endwall is movable on slide rails to allow easy accesses to the test cascades and has a three-dimensional traverse device with four pulse motors. The device includes a rotatable window on which a five-hole pitot microprobe with head size of 1.5 mm is fixed. The probe can be moved to any measurement point before, within, and after the test cascade and can be rotated around the probe axis. These traverse movements and the pressure data acquisition are controlled by a computer system. The displacement error of the traverse gear and angle error are approximately ± 0.01 mm and ± 0.05 deg, respectively. The cascade outlet velocity was set by a Prandtl-type total/static pressure probe located far downstream of the test cascade.

Figure 2 shows the test blade profile, where the profile coordinates can be found in Ref. 4. The cascades presently tested are straight blade cascade (bowed angle of 0 deg), two negative bowed blade cascades with bowed angles (inclining angle at the ends) of -10 and -20 deg, and three positive bowed blade cascades with bowed angles of 10, 20, and 30 deg. The cross-sectional profiles at any blade height parallel to the endwall are the same for all bowed blades. Figures 3 and 4 show three-dimensional views of test blades and blade stacking lines along the blade height, respectively. Here we define positive bowed angle as when the angle between the endwall and blade pressure surface is an acute angle and vice versa for negative

Presented as Paper 2002-0378 at the 40th Aerospace Sciences Meeting, Reno, NV, 14–17 January 2002; received 20 March 2002; revision received 7 April 2003; accepted for publication 9 April 2003.

*Aerospace Special Researcher, Aircraft Propulsion Research Center. Member AIAA.
†Head, Highly-Loaded Turbomachinery Group, Aircraft Propulsion Research Center.
‡Professor, Department of Mechanical Engineering.
§Ph.D. Student, Institute of Engineering Thermophysics.

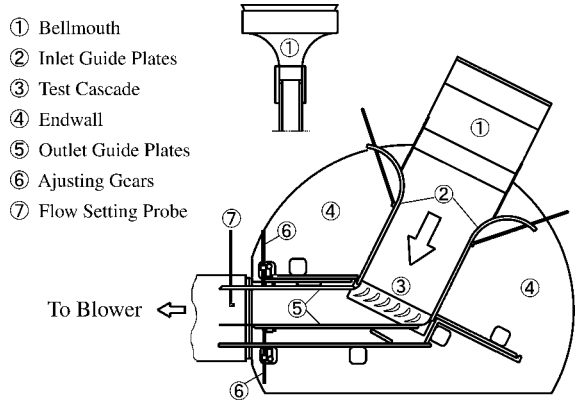

Fig. 1 Cascade wind tunnel.

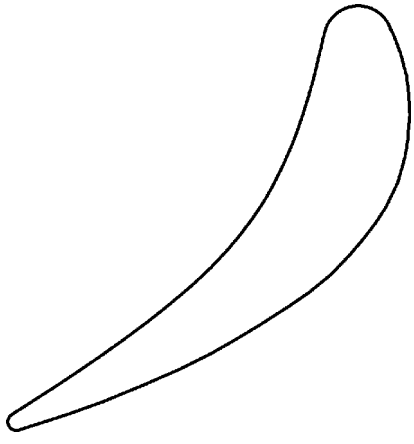

Fig. 2 Blade profile geometry.

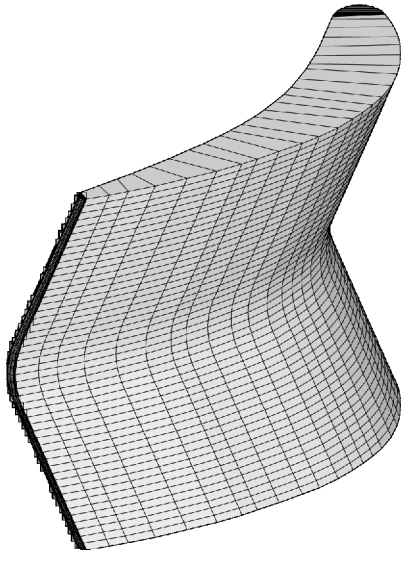

Fig. 3 Three-dimensional view of the bowed blades.

bowed angle. The cascade geometry and aerodynamic parameters are given in Table 1.

The clearance between the movable endwall and blade tip was 1 mm and sealed with felt material, as shown in Fig. 4. The location of two measurement planes are shown by the mesh lines in Fig. 5, and the measurement points on each measurement plane are shown in Fig. 6. In the cascade pitchwise direction, there are 32 points per 1.29 blade pitch and 27 points in the blade height direction. The measurement interval was made finer near both the endwalls as shown in Fig. 6, so that the boundary layer could be more accurately

Table 1 Cascade geometrical and aerodynamic parameters

Parameter	Value
Blade chord C, mm	102.04
Blade pitch T, mm	70.50
Aspect ratio h/C	0.9800
Number of blades N	6
Reynolds number Re	1.8×10^5
Axial blade chord C_{ax}, mm	79.12
Blade height h, mm	101.0
Pitch–chord ratio T/C	0.6909
Cascade inlet flow angle at design $\alpha_{in,d}$, deg	0
Cascade outlet flow angle at design $\alpha_{out,d}$, deg	68

Table 2 Inlet boundary layer parameters

Parameter	Hub	Tip
Boundary-layer thickness δ_{99}, mm	24	22
Displacement thickness δ^*, mm	2.6	2.0
Momentum thickness δ^{**}, mm	2.1	1.7
Shape factor δ^*/δ^{**}	1.2	1.2

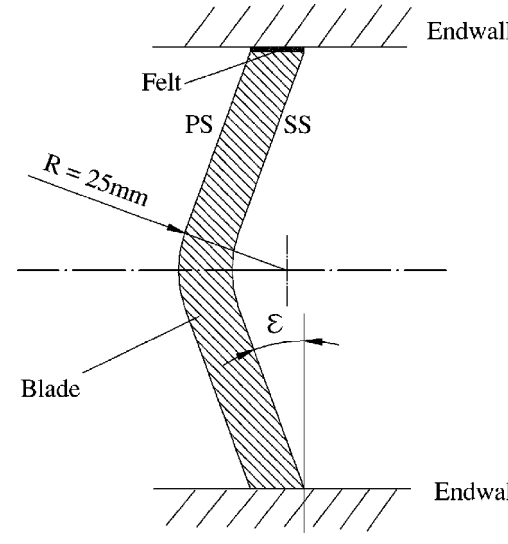

Fig. 4 Bowed blade stacking lines along the blade length.

detected. A boundary-layer trip 5 mm thick and 10 mm wide was attached on both the endwalls at 400 mm upstream to increase the cascade inlet endwall boundary-layer thickness. Table 2 shows some of the cascade inlet boundary-layer parameters. A shape factor of 1.2 (fully turbulent flows at cascade inlet endwalls) is employed for both of the endwall boundary layers. Test cascade outlet Mach number M_{out} is 0.07, and wind-tunnel freestream turbulence intensity T_u is 0.5%.

Analysis Method

In the present analysis, the direction of overall mass-averaged yaw flow angle of each measurement plane is defined as the reference yaw flow direction at each measurement plane. Secondary flow vector $\boldsymbol{V}_s$ is then defined by a projection vector of the local velocity vector $\boldsymbol{V}$ onto the plane normal to the reference yaw flow direction and vertical to the endwalls. The secondary flow vector can be decomposed into two components: $\boldsymbol{v}$ parallel to the endwall plane and $\boldsymbol{w}$ along the blade length. In Fig. 7, secondary flow vectors are drawn by viewing the vectors from the downstream side of the cascade. Secondary flow vorticity is defined by

$$\Omega = \frac{\Delta w}{\Delta x} - \frac{\Delta v}{\Delta y} \tag{1}$$

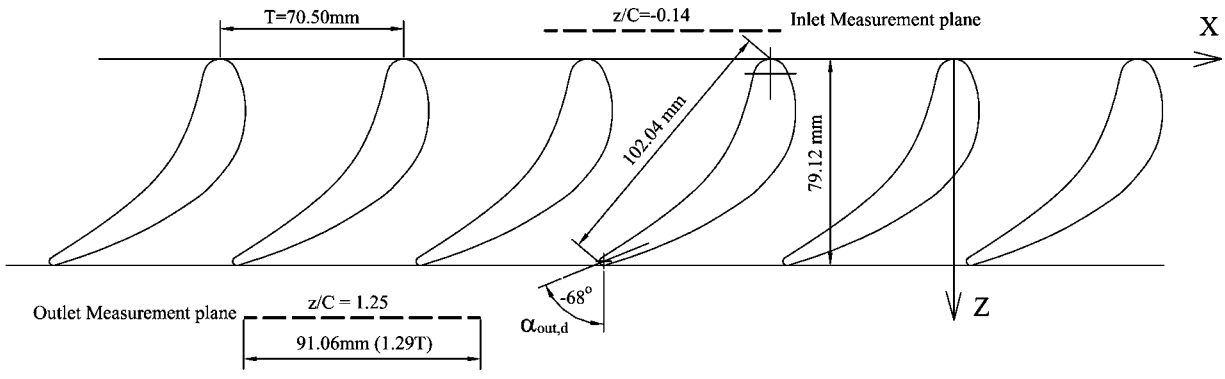

Fig. 5 Location of the measurement planes.

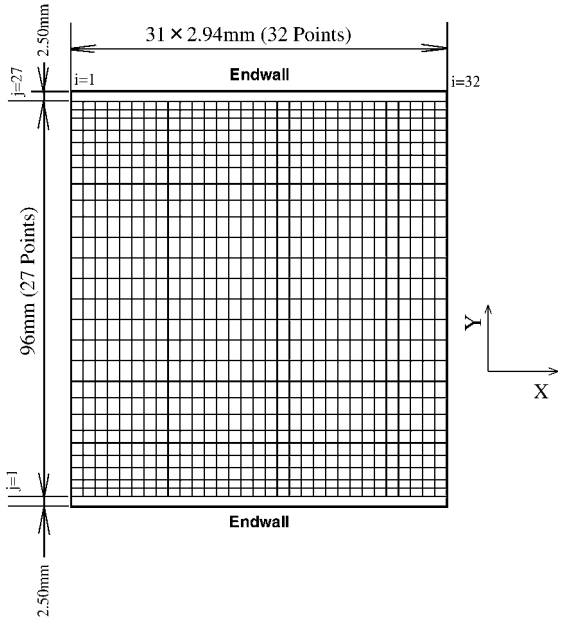

Fig. 6 Distribution of the measurement points.

where Δ is a finite differentiation operator. The total pressure loss coefficient C_{pt} is defined by

$$C_{\text{pt}} = \bar{C}_{\text{pt,mid,st}} - [P_t/(\bar{\bar{P}}_{t,\text{in}} - \bar{\bar{P}}_{s,\text{out}})] \tag{2}$$

where $\bar{\bar{P}}_{t,\text{in}}$ is an overall mass-averaged total pressure at the inlet measurement plane, $\bar{\bar{P}}_{s,\text{out}}$ an overall mass-averaged static pressure at the outlet measurement plane, $\bar{C}_{\text{pt,mid,st}}$ a pitchwise mass-averaged total pressure loss coefficient at the midspan of the inlet measurement plane of straight blade cascade, and P_t the local total pressure.

In the mass-averaging technique, each small control area A_{ij} is formed by four neighboring measuring points. The variables such as the yaw flow angle from the axial direction α, absolute velocity V, axial velocity U, total pressure loss coefficient C_{pt}, etc., of A_{ij} are then arithmetically averaged. In the region near the endwalls, the values on the endwalls are estimated by a linear extrapolation using two experimental data adjacent to each of the endwalls. The pitchwise mass-averaged values at local spans and the overall mass-averaged values of each measurement plane are then computed using the following relations.

Pitchwise mass-averaged values at local spans:

$$\bar{\varphi} = \left[\sum_i (\varphi AU)_{ij}\right]_{j=\text{const}} \Big/ \left[\sum_i (AU)_{ij}\right]_{j=\text{const}} \tag{3}$$

Overall mass-averaged values of measurement plane:

$$\bar{\bar{\varphi}} = \sum_j \sum_i (\varphi AU)_{ij} \Big/ \sum_j \sum_i (AU)_{ij} \tag{4}$$

where φ represents α, V, U, C_{pt}, etc., and i is selected to cover one blade pitch.

Results and Discussion

Secondary Flow Vorticity Contours and Secondary Flow Vectors

Figure 7 shows secondary flow vorticity contours and secondary flow vectors at the outlet measurement plane of some of the test cascades. The vorticity contours can show the magnitude and direction of secondary flows more clearly than the secondary flow vectors, such as passage vortex (PV), trailing vortex (TV), etc., and were used to clarify the flowfields here. For instance, in Fig. 7b for $\varepsilon = 0$ deg, it is easy to find a pair of PVs, PV1 and PV2, and a pair of TVs, TV1 and TV2. These PV1 and PV2 or TV1 and TV2 are symmetrical to the cascade midspan, and their flow directions are opposite to each other. (Negative/positive value indicates clockwise/counterclockwise rotation.) The PVs located near the endwalls are stronger and larger than the TVs. This is a typical secondary flow vorticity distribution for linear turbine stator cascades. In Figs. 7a and 7b, another pair of TVs, TV3 and TV4, are also shown.

If the bowed angle ε changes from 0 to -20 deg or to 30 deg (Fig. 7), the passage vortices can still be seen with approximately the same maximum vorticity, and the effect of blade bowing on this passage vortices is weak. This is different from the results presented in Ref. 12 for turbine rotor cascades with large blade turning angle (about 128 deg), where the positive bowing leads the PVs to strengthen and move toward midspan. The present result is also different from that in Ref. 15 using different stator blade profile (Wang's profile) with nearly the same turning angle (72 deg), where the positive bowing weakened the PVs compared to the 0-deg bowing case. On the other hand, the TVs are affected greatly by the bowing. That is, the positive bowing causes the intensity of TV1 and TV2 to increase and the size to extend to the midspan of the cascade, while causing TV3 and TV4 to disappear. In the case of bowed angle of about 30 deg, the intensity of the TVs exceeds that of the PVs. When the negative bowed angle changes from 0 to -20 deg, TV1 and TV2 decrease in size and move toward the endwalls and vice versa for TV3 and TV4. These behaviors, which are reported to be affected by the bowing, have not been reported by other researchers before.

Total Pressure Loss Coefficient

Figure 8 shows the contours of total pressure loss coefficient at the outlet measurement plane. The loss contour of the straight blade cascade, $\varepsilon = 0$ deg, is similar to conventional turbine stator cascades with low aspect ratio. That is, it is characterized by high-loss cores at the blade suction-side corners near the endwalls. With the bowed angles, $\varepsilon = -20$ or 30 deg, the loss contours roughly follow the blade spanwise stacking line. When the blade bowing changes from

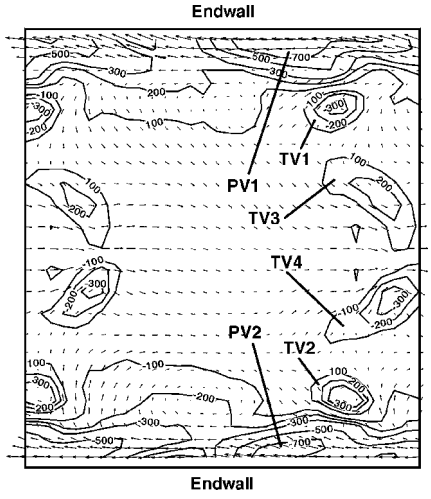

a) $\varepsilon = -20$ deg

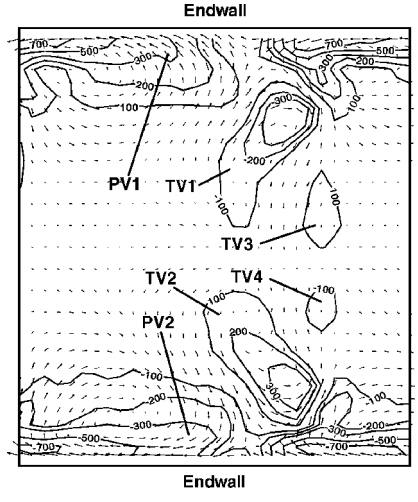

b) $\varepsilon = 0$ deg

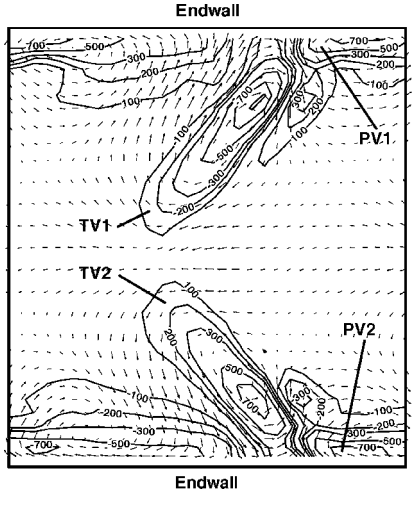

c) $\varepsilon = 30$ deg

Fig. 7 Secondary flow vorticity contours and vectors at the outlet measurement plane.

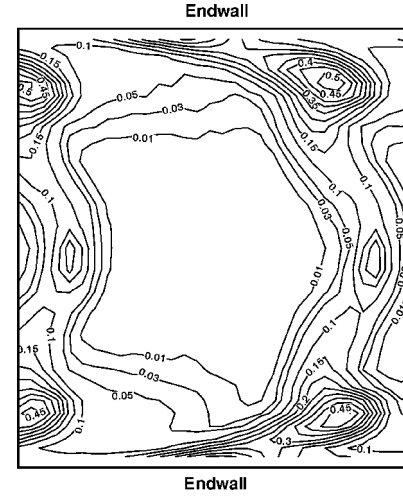

a) $\varepsilon = -20$ deg

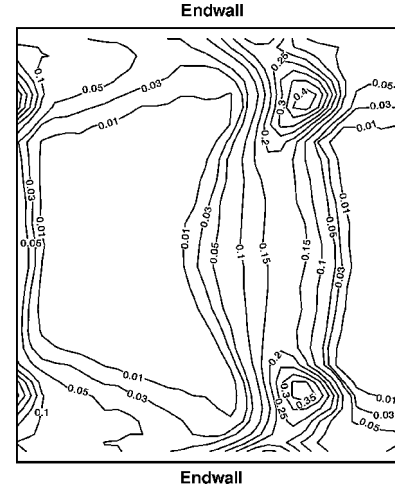

b) $\varepsilon = 0$ deg

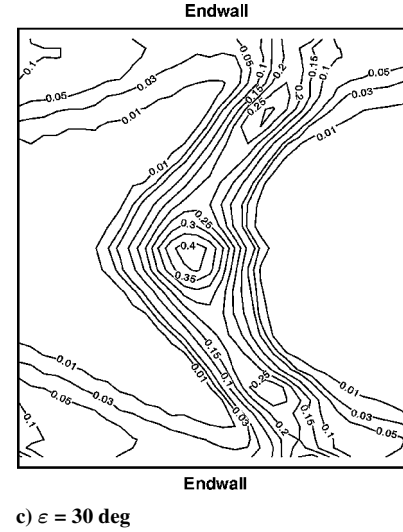

c) $\varepsilon = 30$ deg

Fig. 8 Distribution of the total pressure loss coefficient at the outlet measurement plane.

−20 to 30 deg, the loss around the blade midspan increases, while the loss near the endwalls decreases.

Figure 9 shows spanwise distributions of pitchwise mass-averaged total pressure losses at the cascade inlet and outlet measurement planes. All of the spanwise distributions for bowing angles obtained at the cascade inlet are nearly same. This shows that the cascade inlet boundary-layer profiles were almost unchanged during the test. At the cascade outlet, with increases of bowed angle from −20 to 30 deg, the loss increases in the midspan region (from $H = 22.5 \sim 78.5$ mm) and decreases in the endwall regions ($H = 2.5 \sim 22.5$ mm and $H = 82.5 \sim 98.5$ mm).

The effects of the bowed angle on the overall mass-averaged total pressure loss coefficients at the cascade inlet and outlet measurement planes are presented in Fig. 10. The losses at the cascade inlet, C_{pt1}, are within 0.018 ± 0.002, which corresponds to the inlet boundary-layer losses for all cases. The loss coefficient at the cascade outlet,

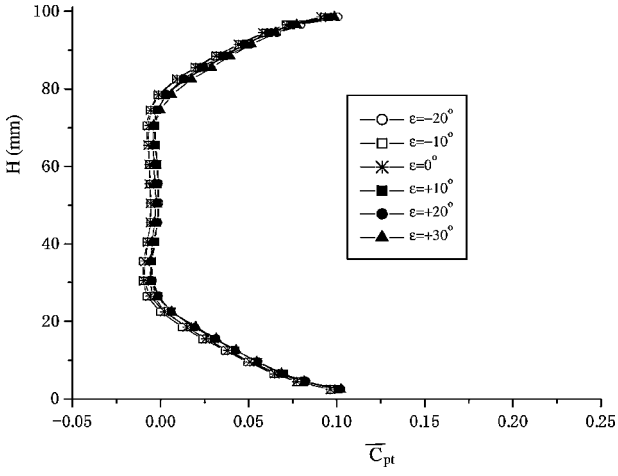

a) Inlet measurement plane

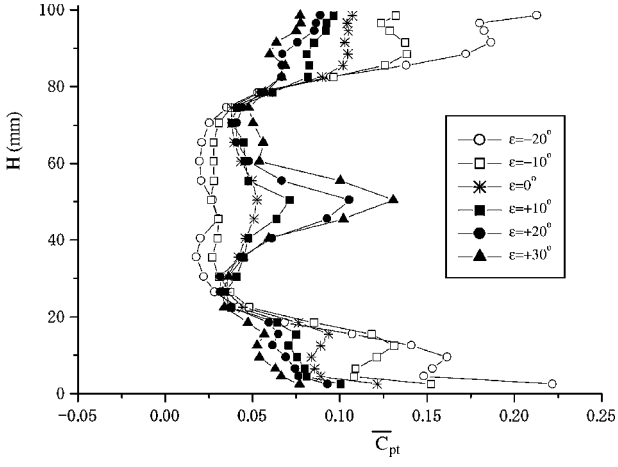

b) Outlet measurement plane

Fig. 9 Spanwise distribution of pitchwise mass-averaged total pressure coefficient.

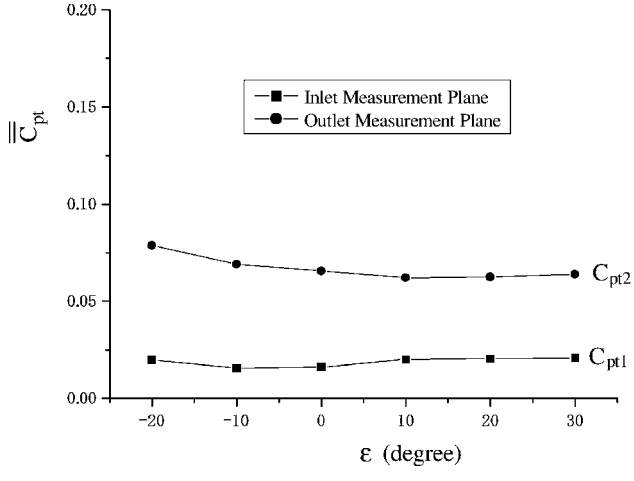

Fig. 10 Variation of overall mass-averaged total pressure loss coefficient with blade bowed angle.

C_{pt2}, is in the range of 0.064 ± 0.002 for positive bowed blade cases. The difference $(C_{pt2} - C_{pt1})$ corresponds to the net loss generated in the cascade passage. The net loss is not particularly affected by the positive bowed angles tested, which is different from the result in Ref. 9, where positive bowed angles ε of 10, 20, and 30 deg reduce the loss coefficient to 32.3%, 41.1%, and 35.4% of the straight cascade, $\varepsilon = 0$ deg, respectively. The negative bowed angles increase the net loss $C_{pt2} - C_{pt1}$.

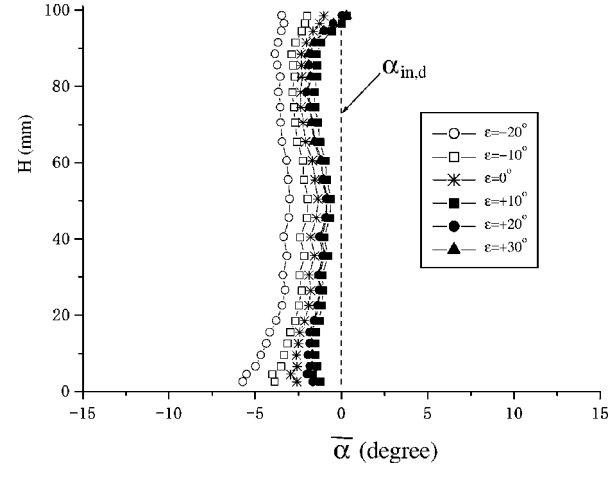

a) Inlet measurement plane

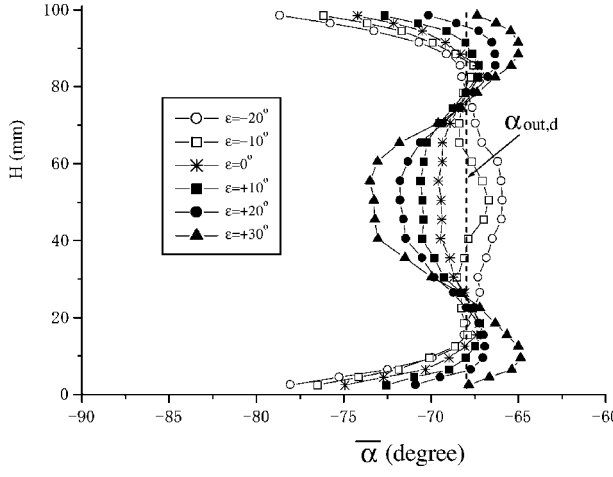

b) Outlet measurement plane

Fig. 11 Spanwise distribution of the pitchwise mass-averaged yaw angle.

Yaw Flow Angles

Figure 11 shows the spanwise distributions of the pitchwise mass-averaged yaw flow angles at the cascade inlet and outlet measurement planes. At the cascade inlet, the yaw flow angle is nearly uniform along the span, but particularly with increases in the bowed angle from 0 to −20 deg. At the cascade outlet, a comparison with straight blade cascade shows that, with increase of the bowed angle from −20 to 30 deg, the yaw flow angle near the endwalls ($H = 2.5 \sim 22.5$ and $82.5 \sim 98.5$ mm) increases, while the yaw flow angle around the midspan ($H = 26.5 \sim 78.5$ mm) decreases. This change in the yaw flow angles is caused by the secondary flows as shown in Fig. 7. Thus, the yaw angle distribution becomes more nonuniform if ε increases. This result is opposite to what was reported in Ref. 9, where the yaw flow angle became more uniform if ε increased close to the physical exit angle of the cascades at the entire blade height.

Figure 12 shows the effects of the bowed angle ε on the overall mass-averaged yaw flow angles at the cascade inlet and outlet. At the inlet, the yaw flow angle is not affected by ε except in negative bowed angle of −20 deg. At the outlet, the effect on the yaw flow angle is also very small, and the yaw angle is between −69.3 and −68.8 deg, which is close to the design yaw flow angle $\alpha_{out,d}$ of −68 deg.

A comparison with two different stator blade profiles (Yamamoto's[4] and Wang's profiles) shows that both the results on the influences of bowing on the cascade flowfields and the performances are different. Furthermore, when the two experiments are compared, it is found that in the experiments of Refs. 9 and 15 the tailgates (endwall plates at the cascade outlet) only extend 5 mm

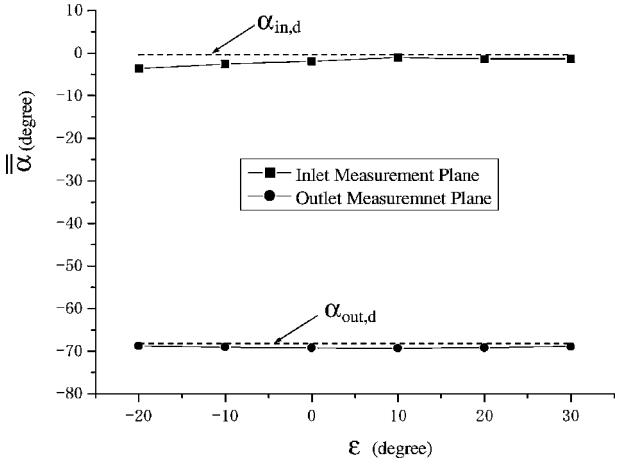

Fig. 12 Variation of overall mass-averaged yaw angle with blade bowed angle.

from the blade trailing edge to downstream, and this is very different from the present cascade setup condition. The influence of the tailgate is reported in Ref. 16, which indicated that the loss near the endwalls decreases significantly when the tailgate was employed. This suggests that the tailgate is very necessary in this kind of experiments.

Conclusions

1) The bowed angle has a significant effect on the secondary flow vortices, such as the TVs, but not on the PVs.

2) The bowed angle significantly affect the spanwise distributions of the loss and the cascade outlet yaw flow angle.

3) The positive bowed angle does not affect the cascade overall flow loss and overall yaw flow angle.

References

[1]Langston, L. S., Nice, M. L., and Hooper, R. M., "Three Dimensional Flow Within a Turbine Cascade Passage," *Journal of Engineering for Power*, Vol. 99, No. 1, 1977, pp. 21–28.

[2]Sieverding, C. H., "Recent Progress in the Understanding of Basic Aspect of Secondary Flows in Turbine Blade Passages," *Journal of Engineering for Gas Turbines and Power*, Vol. 107, No. 2, 1985, pp. 248–257.

[3]Moore, J., and Adhye, R. Y., "Secondary Flows and Losses Downstream of a Turbine Cascade," *Journal of Engineering for Gas Turbines and Power*, Vol. 107, No. 4, 1985, pp. 961–968.

[4]Yamamoto, A., "Production and Development of Secondary Flow and Losses Within Two Types of Straight Turbine Cascades, Part I: A Stator Case," *Journal of Turbomachinery*, Vol. 102, No. 2, 1987, pp. 186–193.

[5]Yamamoto, A., "Production and Development of Secondary Flow and Losses Within Two Types of Straight Turbine Cascades, Part II: A Rotor Case," *Journal of Turbomachinery*, Vol. 102, No. 2, 1987, pp. 194–200.

[6]Deich, M. E., Gubarev, A. B., Filipov, G. A., and Wang, Z. Q., "A New Method of Profiling the Guide Vane Cascades of Turbine Stages with Small Diameter-Span Ratio," *Teploenergetika*, No. 8, 1962, pp. 42–46.

[7]Wang, Z. Q., Lai, S. K., and Xu, W. Y., "Aerodynamic Calcultion of Turbine Stator Cascade with Curvilinear Leaned Blades and some Experimental Results," 5th International Symposium on Air Breathing Engines, No. 30, Feb. 1981, pp. 1–9.

[8]Wang, Z., Han, W., and Xu, W., "The Effect of Blade Curving on Flow Characteristics in Rectangular Turbine Stator Cascades with Different Incidences," American Society of Mechanical Engineers, ASME Paper 91-GT-60, June 1991.

[9]Wang, Z., Han, W., Xu, W., and Zhao, G., "The Blade Curving Effects in a Turbine Stator Cascade with Low Aspect Ratio," *Journal of Engineering Thermophysics* Vol. 11, No. 3, 1990, pp. 160–167 (in Chinese); also Rept. AD-A261 063, Foreign Aerospace Science and Technology Center, Dayton, OH, Jan. 1993.

[10]Shi, J., Han, J., Zhou, S., Zhu, M., Zhang, Y., and She, M., "An Investigation of a Highly Loaded Transonic Turbine Stage with Compound Leaded Vanes," *Journal of Engineering for Gas Turbines and Power*, Vol. 108, April 1986, pp. 265–269.

[11]Harrison, S., "The Influence of Blade Lean on Turbine Losses," *Journal of Turbomachinery*, Vol. 114, No. 1, 1992, pp. 184–190.

[12]Han, W., Wang, Z., Tan, C., Shi, H., and Zhou, M., "Effects of Leaning and of Blades with High Turning Angles on the Aerodynamic Characteristics of Turbine Rectangular Cascades," *Journal of Turbomachinery*, Vol. 116, No. 3, 1994, pp. 417–424.

[13]Wallis, A. M., and Denton, J. D., "Comparison of Design Intent and Experimental Measurements in a Low Aspect Ratio Axial Turbine with Three-Dimensional Blading," American Society of Mechanical Engineers, ASME Paper 98-GT-516, June 1998.

[14]Chen, N., Wang, Z., Wang, S., and Feng, G., "A Study on Secondary Flow Pattern and Blade Bowing Effects in Turbine Bladings," 5th International Symposium on Experimental and Computational Aerothermodynamics of Internal Flows, Sept. 2001, pp. 19–43.

[15]Han, W., Zhao, G., Wu, W., and Wang, Z., "Effect of Blade Curving on Vortices Streamwise in Cascade Exit Flow Field," First International Symposium on Experimental and Computational Aerothermodynamics of Internal Flows, No. 10, Beijing, July 1990, pp. 321–325.

[16]Wang, Z., Han, W., and Xu, W., "The Influence of Tailgate on Effect of Blade Curving," *Journal of Engineering Thermophysics* Vol. 12, No. 3, 1991, pp. 269–273 (in Chinese).

R. M. C. So
Associate Editor